Supplement of Geosci. Model Dev., 17, 8751–8771, 2024
https://doi.org/10.5194/gmd-17-8751-2024-supplement

Geoscientific Model Development
Open Access
EGU

Supplement of

Evaluation of global fire simulations in CMIP6 Earth system models

Fang Li et al.

Correspondence to: Fang Li (lifang@mail.iap.ac.cn)

Supplement

Table S1. Regional annual burned area averaged over 2001–2014 (Mha yr^{-1}).

	BONA -W	BONA -E	TENA -W	TENA -E	CEAM	NHSA	ARCD	SARC	EURO	MIDE	NHAF	SHAF	BOAS	CEAS	SEAS /EQAS	AUST
GFED5	3.2	0.9	2.0	4.0	9.3	9.0	36.9	18.5	3.9	2.7	246.3	234.6	50.5	31.4	56.8	53.6
FireCCI5.1	1.7	0.6	1.5	1.4	1.7	5.5	21.2	5.3	1.5	1.2	152.9	161.4	25.5	16.0	14.1	45.1
MODIS C6	1.6	0.6	1.3	1.2	1.9	5.3	21.2	8.3	0.8	1.2	130.2	149.5	14.4	16.4	13.2	48.6
CMIP5-MME	3.6	2.0	10.4	2.9	4.9	8.9	19.0	10.2	3.1	2.6	10.0	17.6	7.2	5.7	9.5	24.2
CMIP6-MME	2.3	1.9	6.4	5.0	10.3	9.3	53.0	23.7	7.4	8.2	81.4	97.7	14.1	17.0	16.8	40.9
CESM2	0.8	0.3	3.9	2.7	10.3	4.3	73.7	26.6	7.2	6.0	100.0	122.1	10.6	19.5	22.3	36.4
CESM2-WACCM	0.6	0.3	4.4	3.3	11.7	4.2	73.8	28.2	7.2	6.2	103.3	129.1	8.8	20.5	21.6	34.8
CMCC-CM2	6.6	6.1	9.5	16.2	13.8	13.1	61.8	26.1	15.6	4.4	82.1	75.7	35.4	21.8	17.9	33.1
CMCC-ESM2	4.2	2.7	7.8	11.6	12.4	11.4	53.8	23.3	14.6	4.6	81.4	78.5	32.0	20.2	21.5	32.1
CNRM-ESM2	4.7	6.5	19.4	4.6	24.0	19.6	99.6	48.1	4.7	9.7	82.0	213.0	15.7	14.7	10.9	108.6
EC-Earth3-CC	0.8	0.3	3.5	0.6	3.6	12.1	12.6	3.9	1.1	16.4	36.5	19.0	2.1	9.4	9.7	32.0
EC-Earth3-Veg	0.9	0.3	3.1	0.6	3.7	12.5	13.1	3.2	1.0	15.6	37.5	19.7	2.1	7.8	9.4	30.5
NorESM2-LM	0.5	0.1	2.9	2.0	4.9	3.0	31.7	26.1	7.9	5.4	102.4	99.1	5.1	16.3	15.4	26.8
NorESM2-MM	1.3	0.4	3.3	2.8	8.2	3.2	56.4	28.1	7.2	5.3	107.9	123.4	14.9	22.4	22.9	33.4

Table S2. Regional annual fire carbon emissions averaged over 2003–2014 (Tg C yr^{-1}).

	BONA -W	BONA -E	TENA -W	TENA -E	CEAM	NHSA	ARCD	SARC	EURO	MIDE	NHAF	SHAF	BOAS	CEAS	SEAS /EQAS	AUST
GFED4s	45.2	15.4	9.4	7.7	22.8	26.6	251.2	36.3	5.5	1.5	410.6	648.5	126.9	38.9	201.8	91.5
FEER	34.3	7.3	33.5	36.0	75.4	89.3	497.6	136.8	14.4	16.3	719.8	1064.4	208.3	143.9	319.1	210.6
GFAS	58.2	22.1	23.3	15.0	28.9	30.9	238.0	67.2	5.6	8.6	382.2	514.9	211.0	60.6	193.4	132.3
CMIP5-MME	33.1	22.4	89.4	47.3	43.7	116.7	428.4	116.9	31.3	19.6	312.3	286.5	61.1	75.0	149.7	141.8
CMIP6-MME	64.5	35.6	52.4	45.4	54.6	95.8	400.1	117.3	50.8	23.8	277.6	422.0	167.1	89.0	168.1	89.5
AWI-ESM	30.9	18.0	56.8	92.4	54.1	16.9	183.4	93.8	79.7	30.4	261.6	460.9	108.6	111.7	155.5	46.6
CESM2	15.4	3.9	11.6	12.0	68.8	46.2	518.4	150.4	37.7	21.8	290.5	478.4	100.3	87.8	235.8	83.1
CESM2-WACCM	13.9	4.0	12.5	14.2	66.8	55.0	503.4	160.0	39.0	23.2	295.0	489.8	87.6	94.8	245.1	94.9
CMCC-ESM2	41.5	32.3	24.3	54.3	40.5	38.0	188.9	80.3	51.2	7.6	191.0	158.5	140.4	67.6	196.0	45.7
CNRM-ESM2-1	82.0	85.5	97.7	62.7	83.3	61.0	294.1	185.5	71.6	35.5	186.0	603.9	266.7	108.3	55.1	256.6
E3SM1-1	5.5	18.0	21.0	102.7	50.1	35.6	152.2	92.1	66.0	8.6	155.1	161.8	102.9	59.2	111.2	73.3
E3SM1-1-ECA	4.5	4.5	2.3	46.2	31.2	62.7	260.9	60.7	7.7	1.3	235.6	256.9	33.8	35.1	124.2	92.0
EC-Earth3-CC	50.6	18.8	89.2	32.1	78.8	269.4	704.7	141.7	77.1	50.3	614.9	637.3	92.3	117.5	314.1	128.7
EC-Earth3-Veg	61.4	23.7	75.8	33.5	75.5	276.4	706.8	121.7	70.7	49.7	557.5	619.5	102.8	88.4	304.3	131.3
EC-Earth3-Veg-LR	46.3	21.7	74.7	35.8	65.4	293.1	829.2	124.7	62.5	54.0	560.5	616.6	78.2	95.6	258.5	103.9
GFDL-ESM4	73.9	28.1	53.9	128.2	104.0	155.5	763.4	202.8	46.0	15.4	388.2	779.0	142.3	60.6	132.5	83.0
MPI-ESM1-2-HAM	95.1	28.3	155.8	46.6	56.2	30.5	261.2	108.3	39.4	36.4	282.9	624.5	146.2	119.5	95.7	52.2
MPI-ESM1-2-LR	98.8	24.1	146.5	49.3	48.5	17.0	306.5	94.4	54.5	33.6	179.9	473.4	164.3	147.9	89.3	37.2
MRI-ESM2-0	475.9	292.1	56.2	27.6	6.6	12.8	43.7	34.9	108.0	11.8	14.0	31.8	1173.9	186.5	30.0	3.4
NorCPM1	1.9	2.7	18.0	10.0	16.4	89.6	146.4	77.2	9.3	4.0	44.3	99.4	7.1	15.2	42.3	123.3
NorESM2-LM	14.3	2.4	7.2	10.5	46.3	55.2	374.2	137.2	38.5	19.6	291.6	368.5	42.2	70.2	199.6	76.9
NorESM3-MM	24.7	5.3	7.8	14.0	61.3	45.5	480.9	142.1	36.4	18.3	311.7	488.9	135.5	101.4	250.3	99.9
TaiESM1	24.9	27.5	32.4	46.0	29.7	164.1	482.9	103.0	19.9	6.6	136.6	247.1	83.1	34.4	185.6	79.3

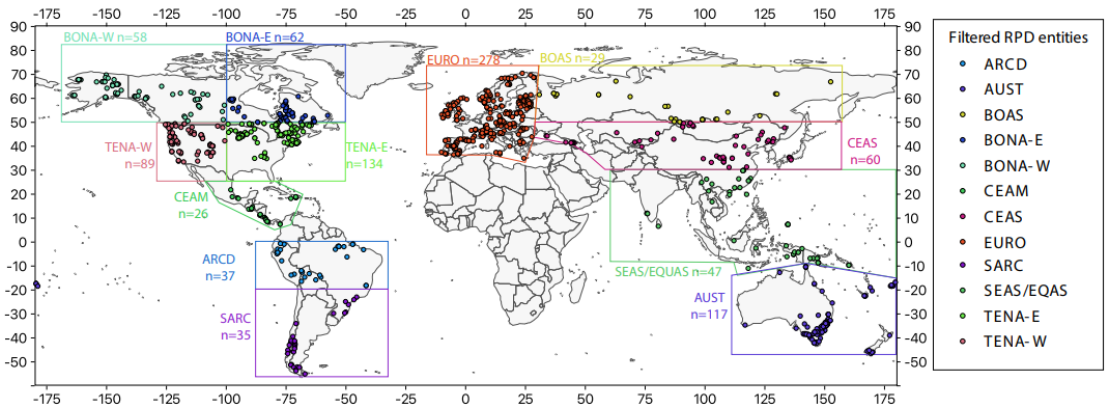

Fig. S1. 992 site locations of charcoal records from Reading Palaeofire Database (RPD) used in this study and regions (enclosed by boxes) where composite time series were constructed.

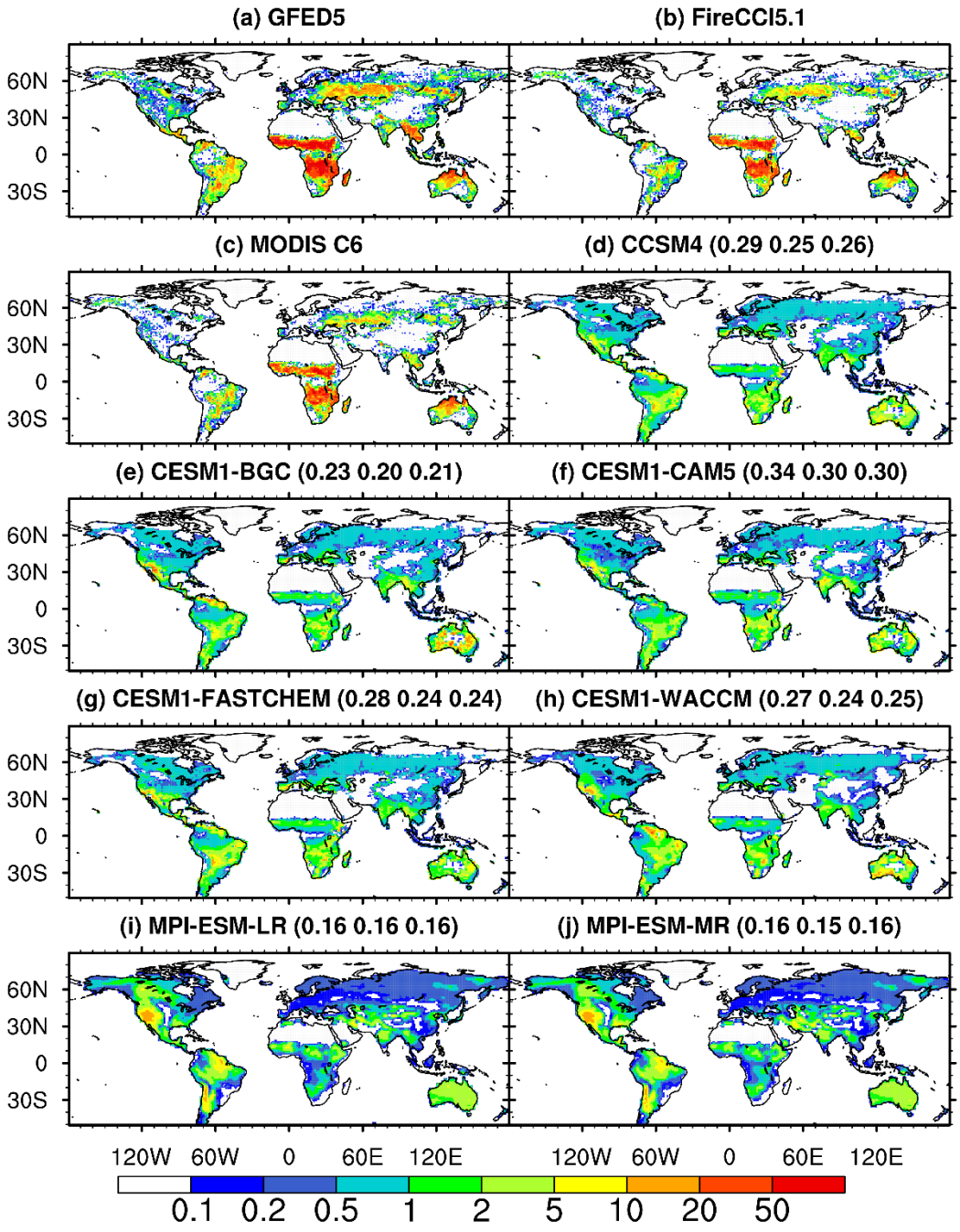

Fig. S2. 2001–2004 spatial distribution of annual burned area fraction (% yr^{-1}) for (a–c) benchmarks and (d–j) CMIP5 models. The spatial correlations of simulations with three benchmarks are also given in parentheses.

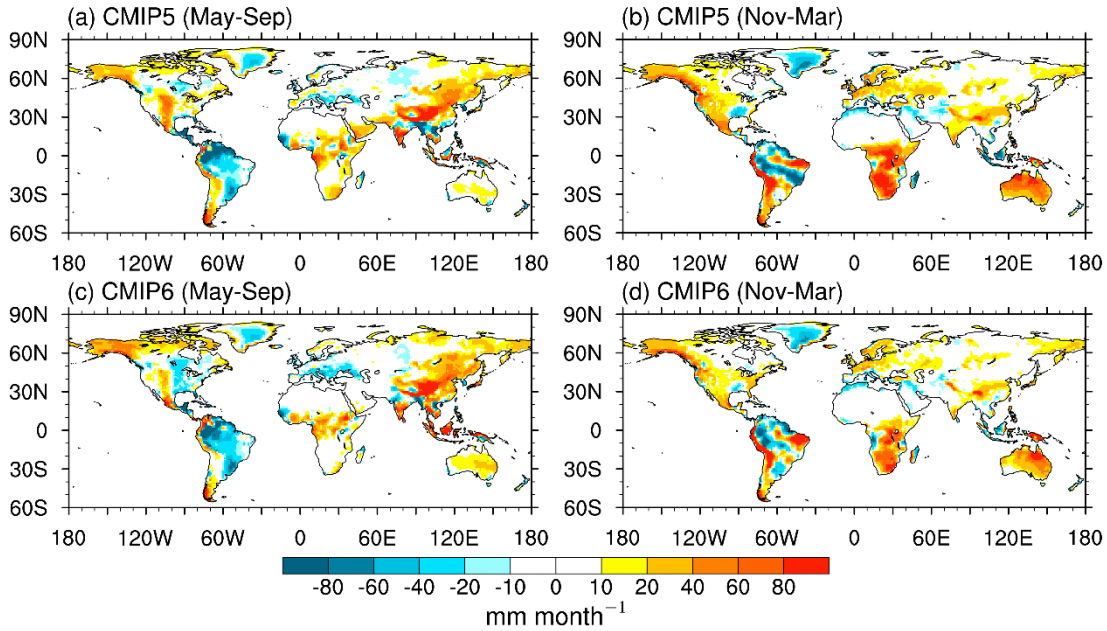

Fig. S3. Simulation bias in monthly precipitation from multi-model ensemble means of CMIP6 models using the Li fire scheme compared to CMIP5 models for 2001–2005. Fire season generally spans May to September for NH mid- (excluding crop fires) and high latitudes and SH tropics, where climate primarily influences fuel wetness. Outside this period, climate impacts fuel availability, a limiting factor in non-forest regions. For the NH tropics and SH mid-latitudes, the situation is reversed, with fire season spanning November to March.

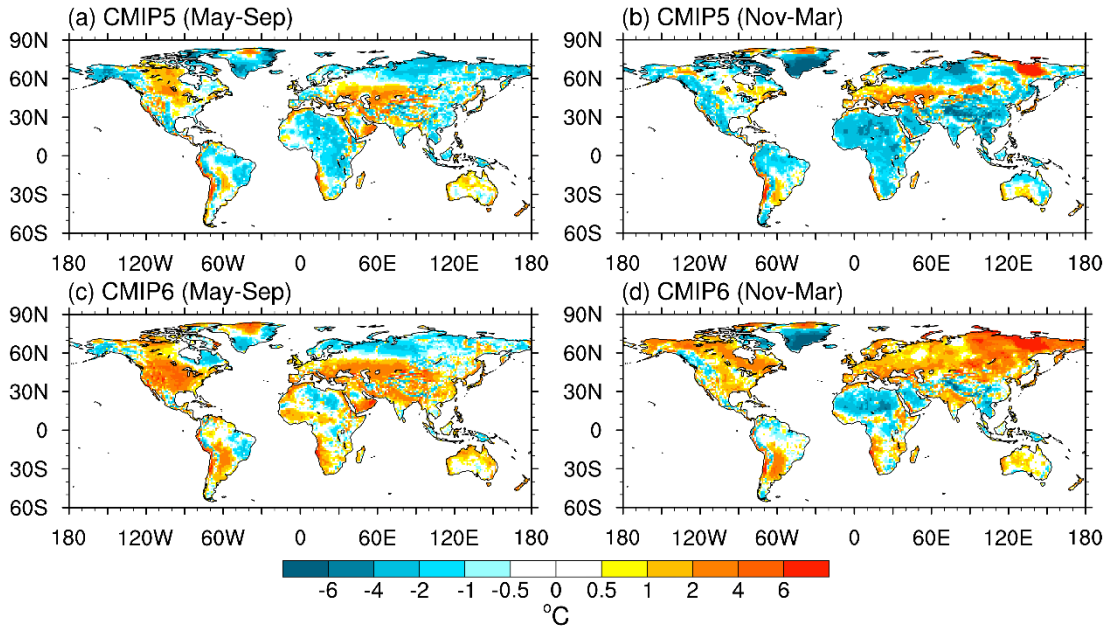

Fig. S4. Same as Fig. S3, but for simulation bias in surface air temperature.

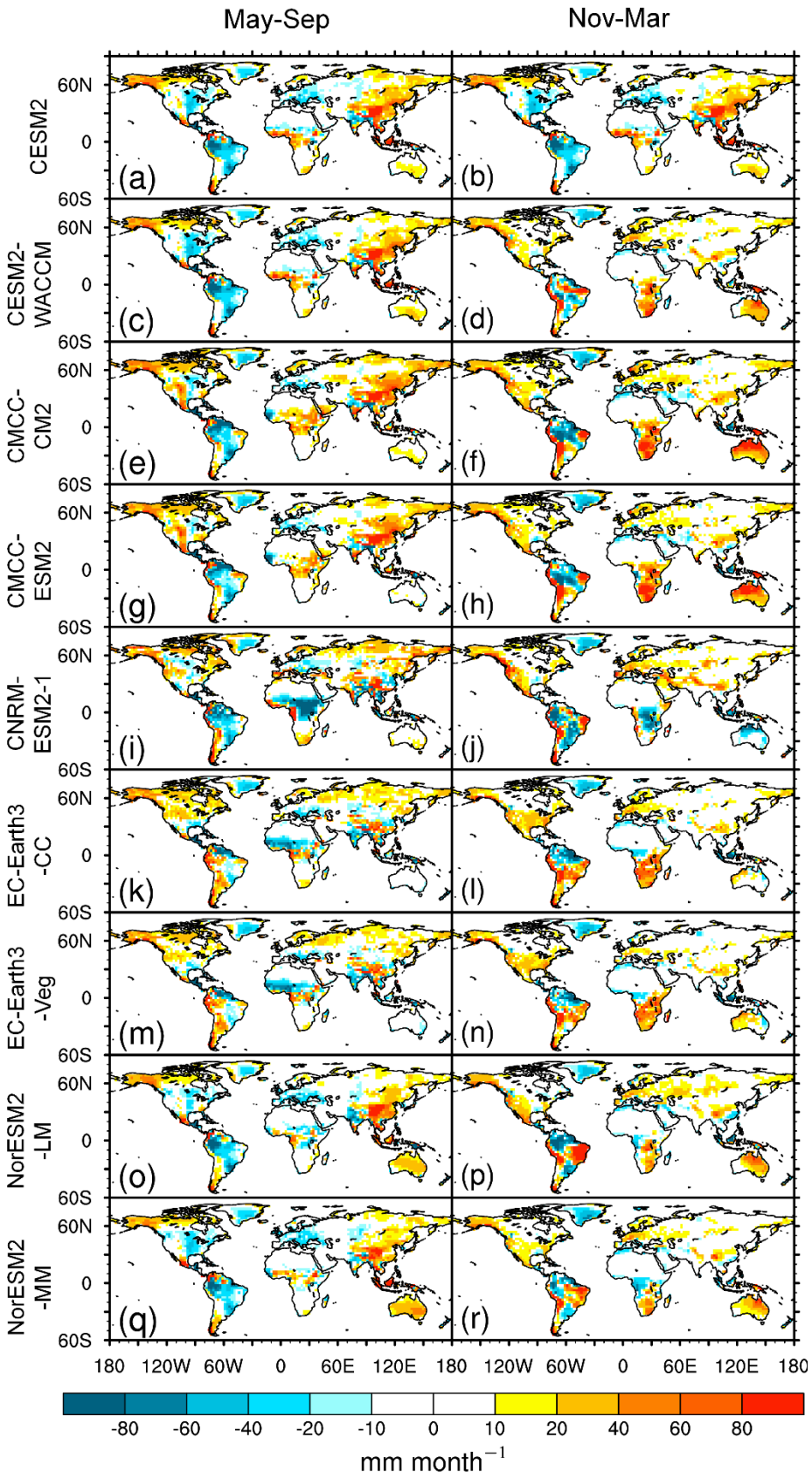

Fig. S5. Same as Fig. S3, but for precipitation simulation bias of each CMIP6 models.

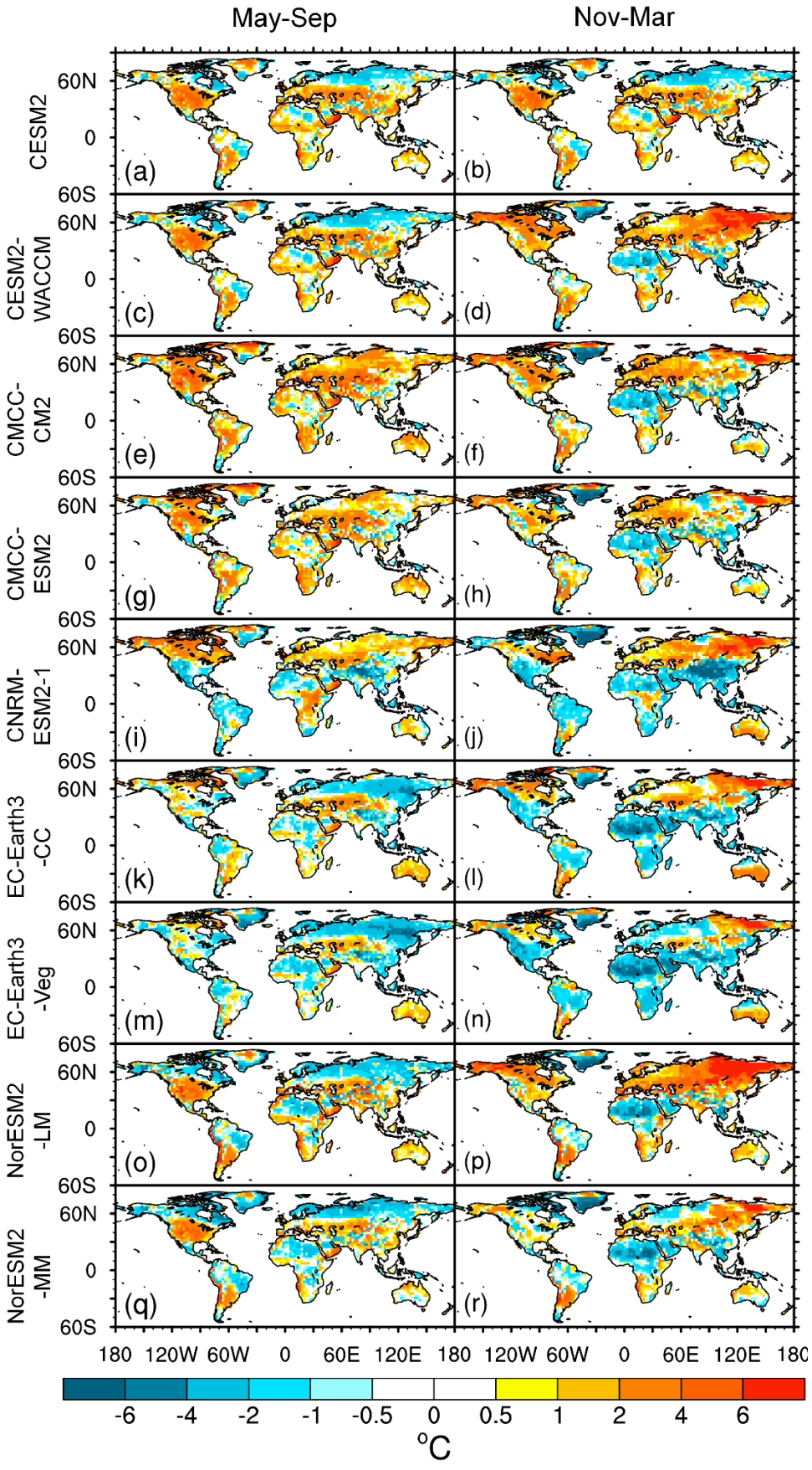

Fig. S6. Same as Fig. S3, but for simulation bias of surface air temperature for each CMIP6 models.

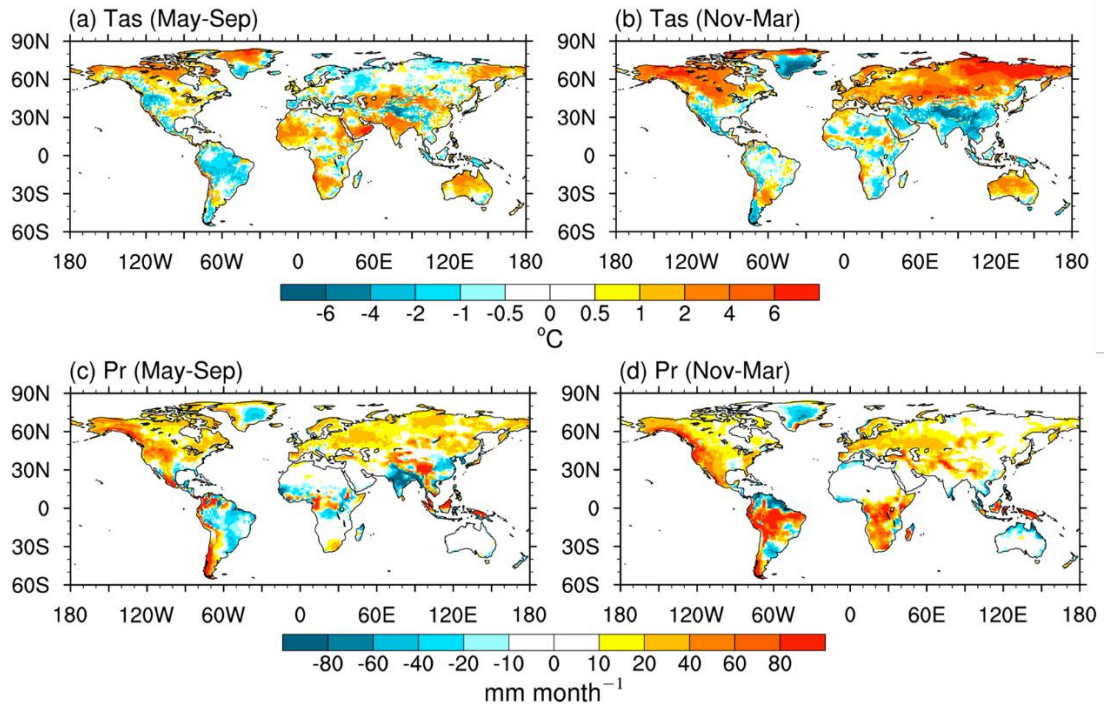

Fig. S7. Same as Fig. S3, but for the simulation bias of MRI-ESM2-0 in (a–b) surface air temperature and (c–d) precipitation for 2003–2014.

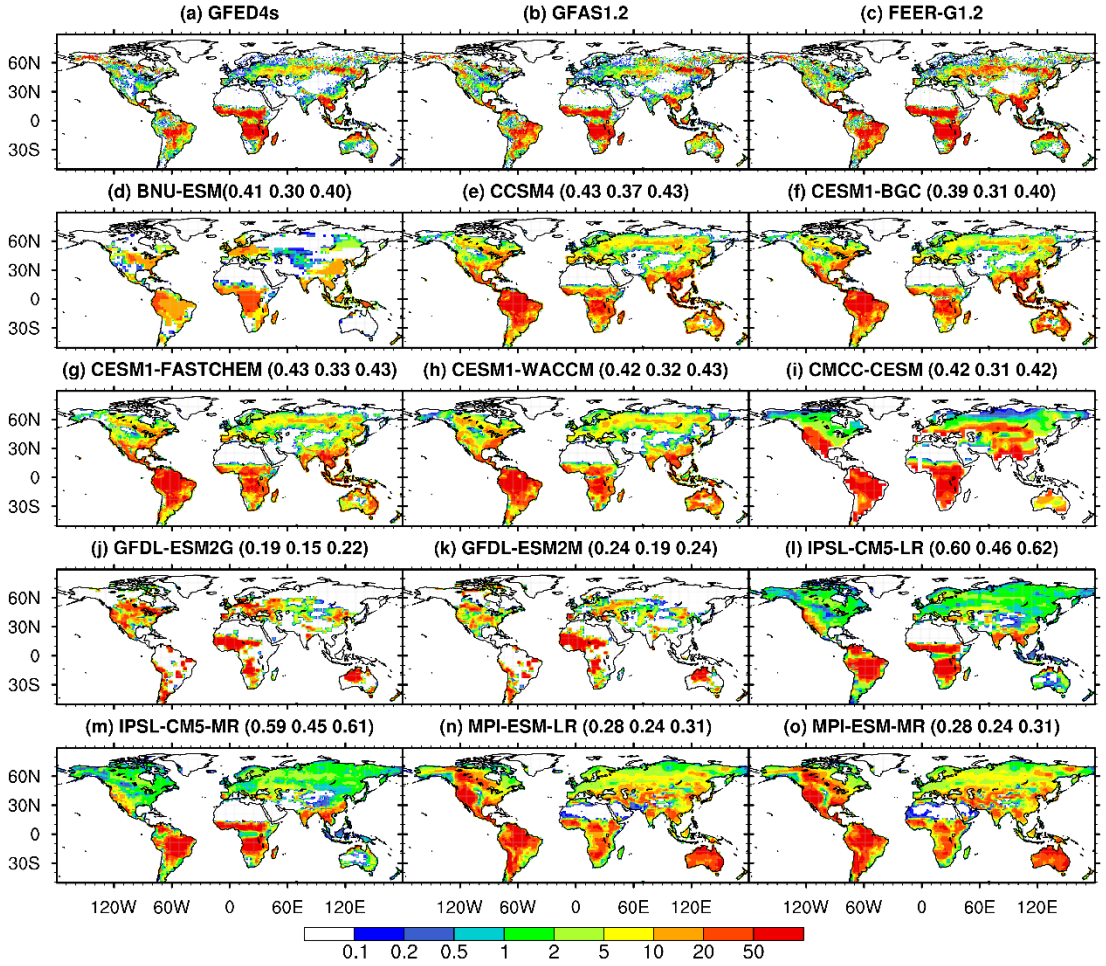

Fig. S8. Same as Fig. S2, but for the 2003–2004 average of fire carbon emissions (g C m^{-2} yr^{-1}).

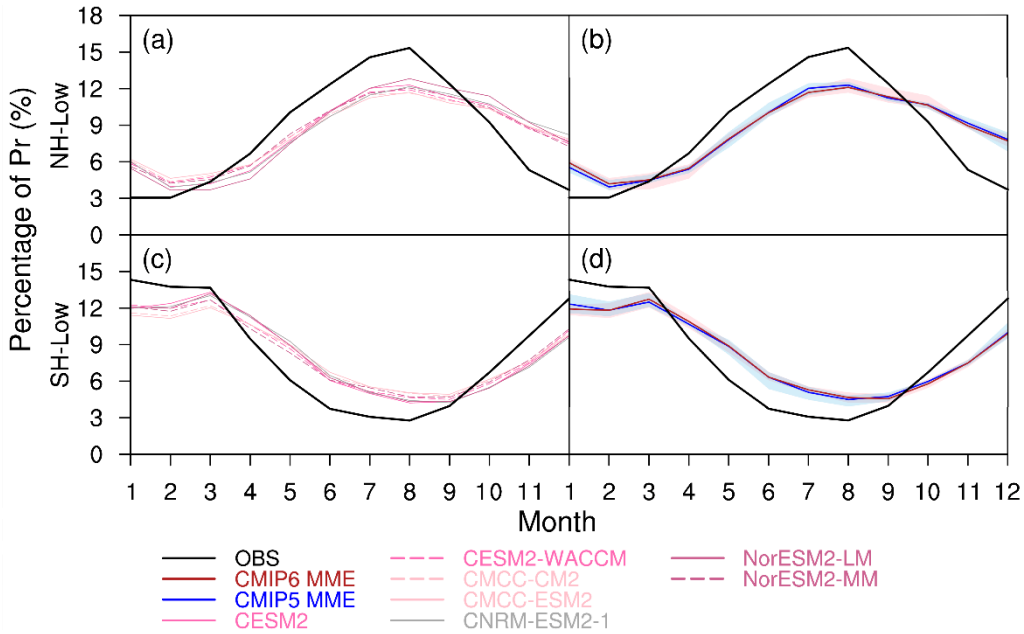

Fig. S9. Seasonal cycle of precipitation in low latitudes for observations and (left) CMIP6 models averaged over 2001–2014 and (right) CMIP6 and CMIP5 multi-model mean (MME) for 2001–2005.

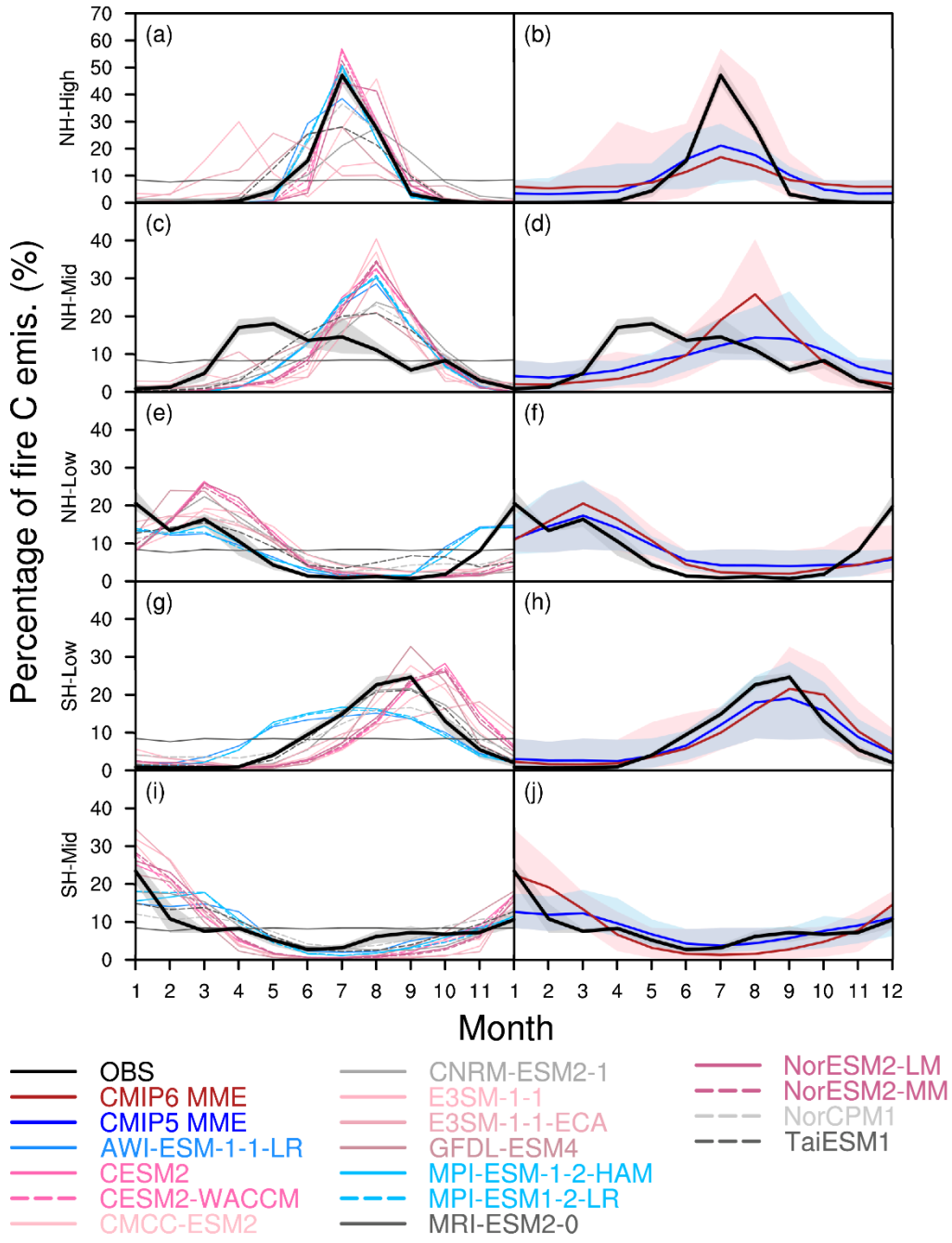

Fig. S10. Seasonal cycle of fire carbon emissions for observations and (left) CMIP6 models averaged over 2003–2014 and (right) CMIP6 and CMIP5 multi-model mean (MME) for 2003–2005. EC-Earth3 models that update fire emissions annually are excluded.

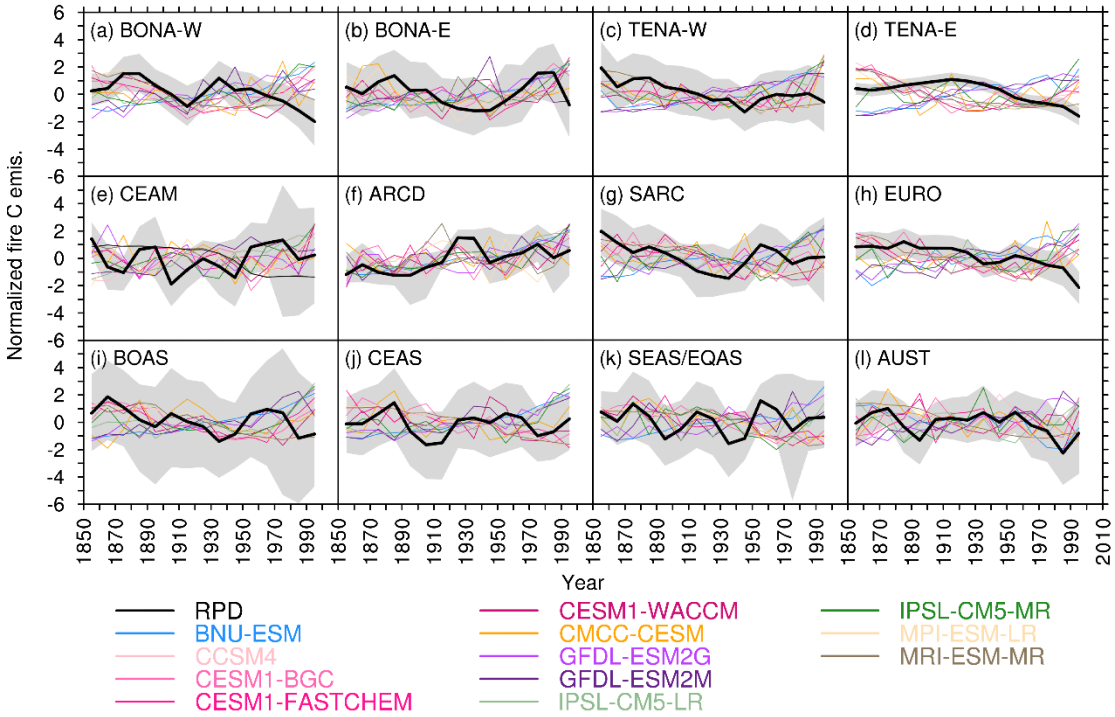

Fig. S11. Standardized fire carbon emissions simulated by CMIP5 models and indicated by RPD charcoal product.

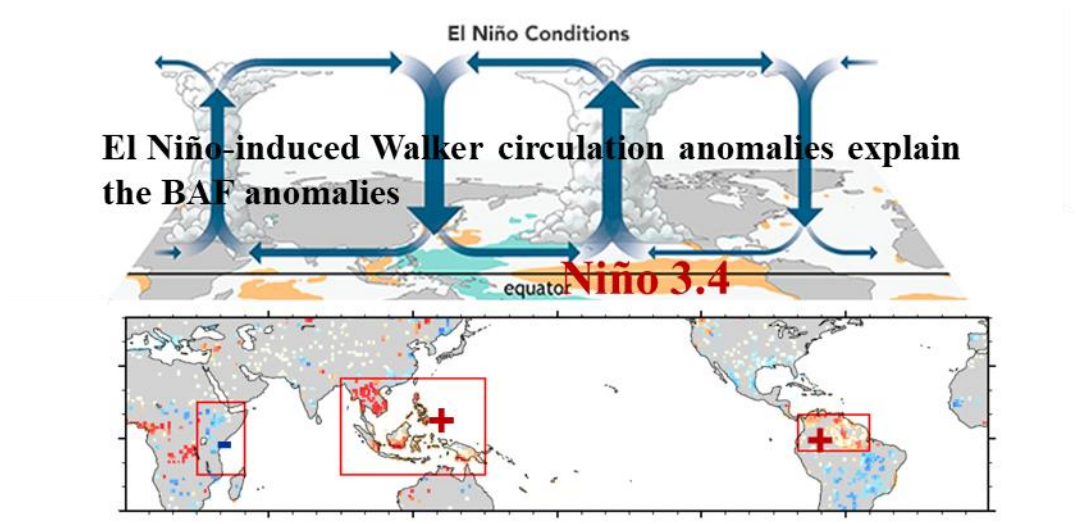

Fig. S12. Influence of ENSO on the burned area. The lower panel shows the regressed coefficient of Jun-May GFED5 BAF anomalies related to the DJF Nino3.4 index from 1997 to 2020. The El Niño event leads to an increase in burned area fraction in equatorial Southeast Asia and South America, while a decrease in eastern Africa, due to the El Niño-induced zonal Walker circulations along the equator.

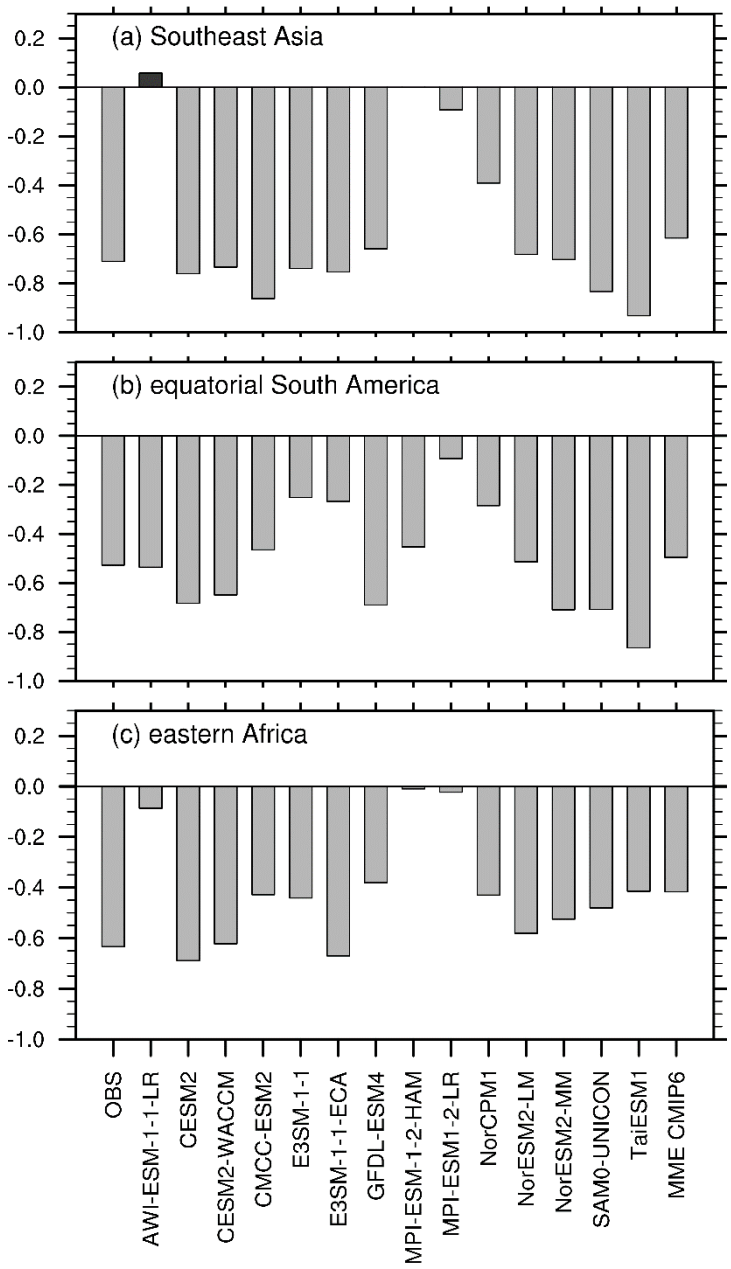

Fig. S13. Similar to Fig. 11, but for correlation coefficient of local fire carbon emissions with precipitation averaged from preceding June to the following May for GFED4s (Obs) for 1997–2019 and CMIP6 models for 1850–2014.

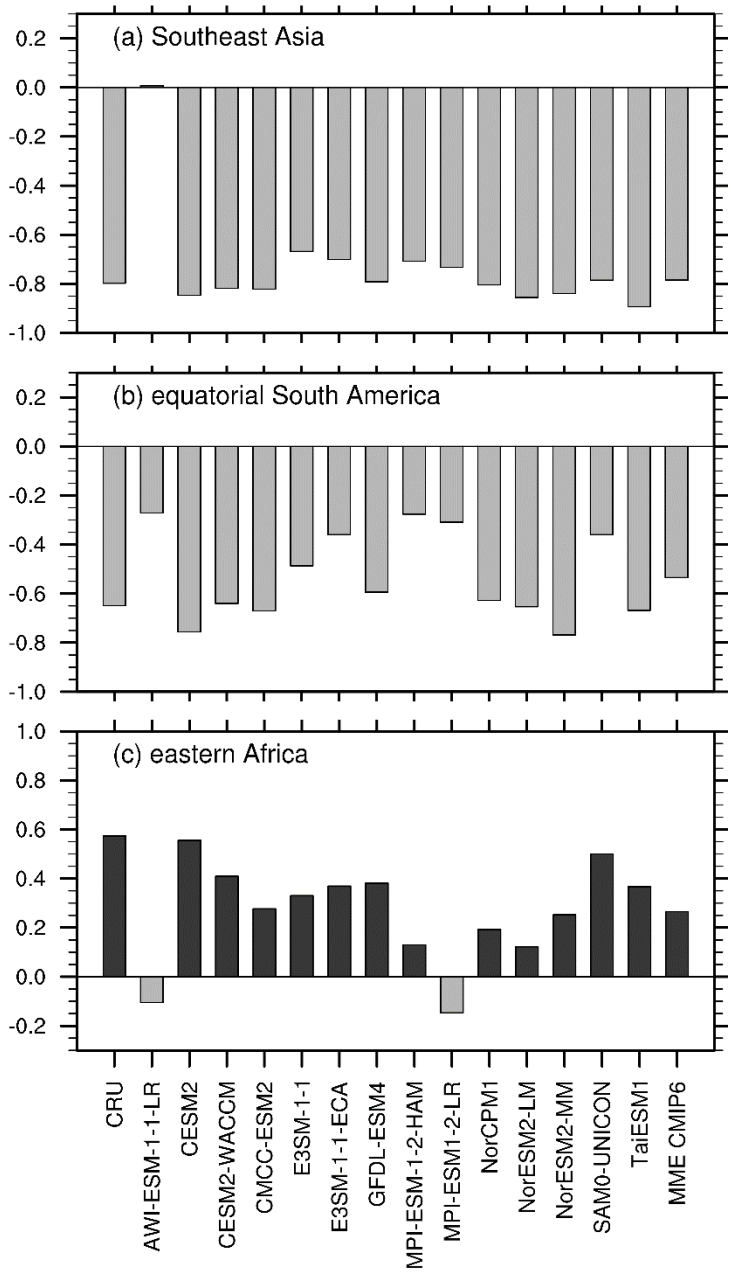

Fig. 14. Same as Fig. S13, but for correlation coefficient of Jun−May averaged precipitation with DJF Niño3.4 index for CRU (1997–2019) and CMIP6 models (1850–2014).

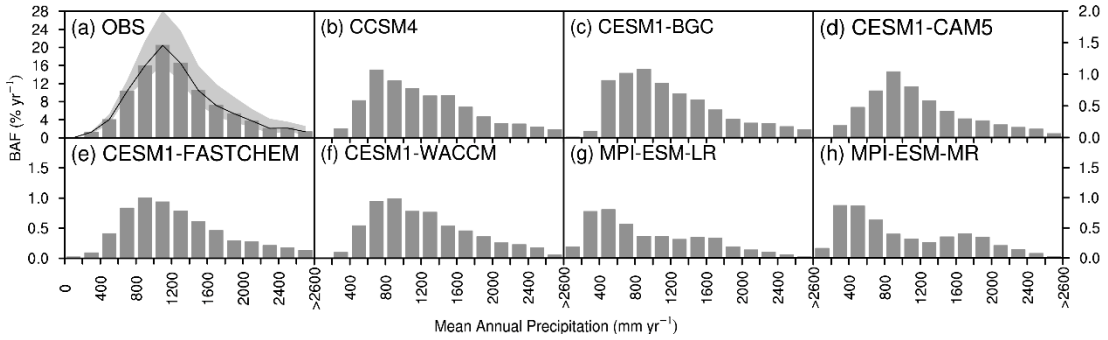

Fig. S15. Burned area fraction between 35°N and 35°S in 200 mm yr^{-1} bin of mean annual precipitation for benchmarks and CMIP5 models.

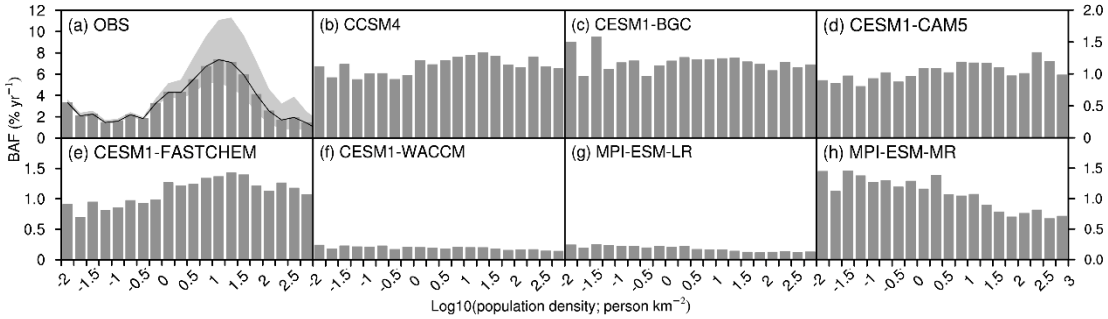

Fig. S16. Burned area fraction changes with increasing population density for benchmarks and CMIP5 models.